Superlocalization of Single Molecules and Nanoparticles in High-Fidelity Optical Imaging Microfluidic Devices

ARTICLE *in* ANALYTICAL CHEMISTRY · JUNE 2011

Impact Factor: 5.64 · DOI: 10.1021/ac201056z · Source: PubMed

5 AUTHORS, INCLUDING:

Yong Luo
Dalian University of Technology
27 PUBLICATIONS **425** CITATIONS
SEE PROFILE

Wei Sun
Washington University
41 PUBLICATIONS **644** CITATIONS
SEE PROFILE

Chang Liu
University of British Columbia - Vancouver
15 PUBLICATIONS **191** CITATIONS
SEE PROFILE

Gufeng Wang
North Carolina State University
53 PUBLICATIONS **1,206** CITATIONS
SEE PROFILE

analytical chemistry

LETTER

pubs.acs.org/ac

Superlocalization of Single Molecules and Nanoparticles in High-Fidelity Optical Imaging Microfluidic Devices

Yong Luo,[†,‡] Wei Sun,[†] Chang Liu,[†,§] Gufeng Wang,[†] and Ning Fang*[,†]

[†]Ames Laboratory, U.S. Department of Energy and Department of Chemistry, Iowa State University, Ames, Iowa 50011

[‡]School of Pharmaceutical Science and Technology, Dalian University of Technology, Dalian, Liaoning, China

[§]Department of Chemistry, University of British Columbia, Vancouver, BC, Canada

Supporting Information

ABSTRACT: Superlocalization of single molecules and nanoparticles with a precision of subnanometer to a few tens of nanometers is crucial for elucidating nanoscale structures and movements in biological and chemical systems. A novel design of ultraflat and ultrathin glass/polydimethylsiloxane (PDMS) hybrid microdevices is introduced to provide almost uncompromised optical imaging quality for on-chip superlocalization and super-resolution imaging of single molecules and nanoparticles under a variety of microscopy modes. The performance of the high-fidelity (Hi-Fi) optical imaging microfluidic device was validated by precisely mapping micronecklaces made of fluorescent microtubules and 40 nm gold nanoparticles and by demonstrating the activation and excitation cycles of single Alexa Fluor 647 dyes for direct stochastic optical reconstruction microscopy in PDMS-based microchannels for the first time. Furthermore, the microdevice's feasibility for multimodality microscopy imaging was demonstrated by a vertical scan of live cells in epi-fluorescence and differential interference contrast (DIC) microscopy modes simultaneously.

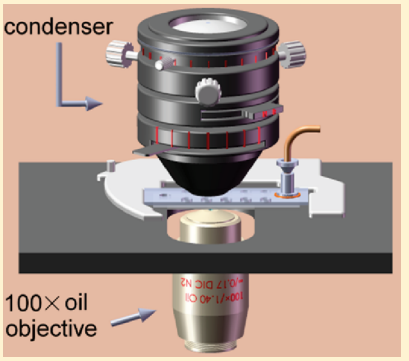

The understanding of cellular processes and molecular biophysics has been greatly expanded in the past 2 decades, largely owing to the discoveries of a variety of contrast agents, including green fluorescent protein (GFP) and its numerous variants,[1,2] quantum dots,[3] and plasmonic nanoparticles,[4] and the developments of optical imaging tools for visualizing these probes with high sensitivity and sufficient spatial and temporal resolution.[5−13] Superlocalization of single molecules and nanoparticles with a precision of subnanometer to a few tens of nanometers is crucial for elucidating nanoscale structures and movements in biological and chemical systems. For example, stochastic optical reconstruction microscopy (STORM),[14,15] as well as photoactivated localization microscopy (PALM),[16,17] realizes the high resolution by superlocalizing randomly activated photoswitchable fluorophores, and their effective spatial resolution is governed by the signal-to-noise ratio (SNR) for the detection of single fluorophores; differential interference contrast (DIC) and dark field microscopies have been employed successfully to trace nanoparticle probes to reveal motions induced by kinesin motor proteins.[13,18,19]

An essential assumption of the superlocalization-based studies is that the recorded locations and movements of single molecules and nanoparticles can faithfully represent their actual locations and movements in the sample. Herein, the faithful optical recreation of the sample with high sensitivity and resolution is referred to as high-fidelity (Hi-Fi) optical imaging. The assumption of Hi-Fi optical imaging is generally valid when the sample is prepared in the standard sandwiched "slide-specimen-coverslip" configuration for imaging under light microscopes.

In parallel with the developments in imaging techniques, microfluidics has grown into an enormous research field crossing over chemistry, biology, materials, and microelectronics.[20−22] The platforms used in single molecule and nanoparticle studies are migrating from standard microscope sample slides, chambers and flow cells with simple channel designs to microfluidic devices with more complex 2D or 3D channel networks and integrated functional elements for controlled delivery of mechanical, thermal, electrical, and optical stimuli.[23−33]

Microfluidic devices made of polydimethylsiloxane (PDMS) elastomer and cover glass are widely considered the choice of design for on-chip optical imaging, due to a number of well-known features, including optical transparency, PDMS's permeability to oxygen and carbon dioxide to allow long observation time of live biological samples, flexible and versatile channel layouts for a wide range of applications, and low-cost and accessible microfabrication. However, it is still challenging to accomplish Hi-Fi optical imaging in certain microscopy modes on these microfluidic devices, due to the restrictions of the material, structure and size of microdevices, and the limitations imposed by various microscopy modes.

For a far-field microscopy mode that uses the same objective for illumination (excitation) and detection, such as confocal fluorescence microscopy and objective-type total internal reflection

Received: April 25, 2011
Accepted: June 7, 2011
Published: June 07, 2011

fluorescence microscopy (TIRFM), ultrasensitive single molecule detection can be realized on typical PDMS-coverslip microfluidic devices as the excitation and emission light passes through only a single piece of cover glass between the sample and the objective.[34,35]

For other far-field microscopy modes that do not use the same objective for illumination and detection, such as transmitted-light DIC microscopy and prism-type TIRFM, the current designs of PDMS-coverslip microfluidic devices cannot produce the same Hi-Fi image quality as the standard microscope sample slide due to the requirements on the thickness and optical quality of the sample slide. In DIC microscopy, the typical maximum thickness of the sample slide for a set of 100 × 1.4 numerical aperture (N.A.) oil-immersion objective and condenser is ~1.3 mm, which is calculated as the sum of the glass slide thickness of 1 mm, the no. 1.5 coverslip thickness of 0.17 mm, and the objective working distance of 0.13 mm. A similar requirement of the sample slide thickness applies to imaging on prism-type TIRFM. At such thickness (from tens to a few hundreds of micrometers), the PDMS layer lacks mechanical stability and is hard to bond with the coverslip homogeneously. Thus, it is difficult to make all of the surfaces of the optically transparent building blocks flat and parallel to each other using the classical replica molding process.[36] (See the Supporting Information for detailed discussion.) The reduced optical imaging quality results in higher background noise and more significant interference fringes, which in turn lead to lower accuracy and precision in superlocalization.

Herein, we modified the classical replica molding process to create a new type of Hi-Fi microfluidic device specifically for the applications that need superlocalization of single molecules and nanoparticles in microchannels. This three-layer device uses a standard microscope slide and a coverslip to sandwich an ultrathin PDMS layer without causing deformation to any surface in the optical path. The structural similarity warrants the new microdevice's applicability under most (if not all) types of optical microscopies that are compatible with the standard "slide-specimen-coverslip" configuration.

The ultraflat and ultrathin PDMS layers are fabricated following a modified procedure (Figure 1) based on the classical replica molding,[36] thus can be made in any microfabrication laboratory with basic equipments at a low cost. The thickness of the PDMS layer is precisely controlled by two identical spacers (3 M double-sided tapes of various thicknesses) placed between a microscope glass slide and a master, which is a piece of SU8-patterned Si wafer or microscope slide. The top and bottom faces of the PDMS layer cured between the glass slide and the master are flat and parallel to each other. The surface of the glass slide is unmodified whereas the master is modified with (tridecafluoro-1,1,2,2-tetrahydrooctyl)-1-trichlorosilane. The thin PDMS layer is peeled off from the master in step 7, but it remains attached securely to the glass slide and maintains its mechanical stability and structure. The PDMS layer is then homogeneously bonded with a piece of coverslip to form the microchannels in the sandwich. Besides the holes drilled at the channel ends, there are additional holes in the glass slide to function as windows through which the living biological samples in the microchannels can communicate with the outer environment to keep their viability.

The performance of the Hi-Fi optical imaging microchannels was validated by precisely mapping micronecklaces made of fluorescent microtubules and 40 nm gold nanoparticles and by demonstrating the activation and excitation cycles of single Alexa Fluor 647 dyes in PDMS-based microfluidic channels.

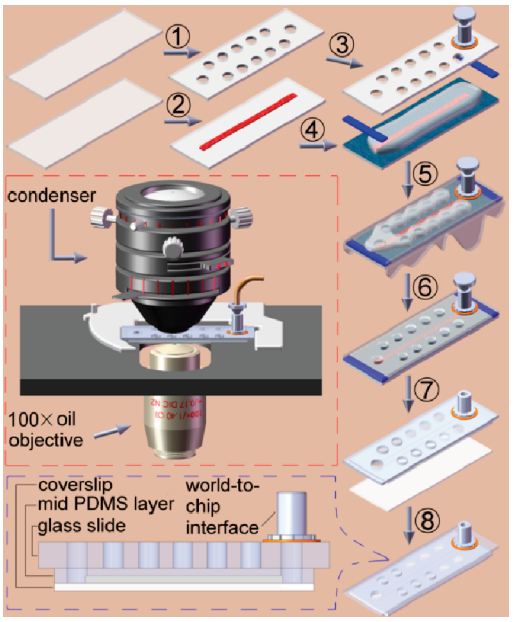

Figure 1. Fabrication procedure for the glass/PDMS hybrid microdevice suitable for high-fidelity optical imaging: (1) drill holes on a glass slide according to the microchannel network design; (2) fabricate the master by patterning SU8 on another glass slide; (3) fabricate world-to-chip interface on the glass slide; (4) modify the master surface with silane indicated by the blue texture; (5) assemble the glass slide with holes and interface on, the spacers, and the modified master with PDMS prepolymer poured on and cure the assembly; (6) remove the excess polymerized PDMS on the top and sides; (7) detach the master, spacers, and interface cap from the assembly and drill holes at the channel ends; (8) attach coverslip to the remaining assembly to form the final sandwich microdevice. The blue dashed box highlights the side view of the final microdevice. The red dashed box shows the microdevice on an inverted microscope.

The micronecklaces were formed by binding 40 nm gold nanospheres to fluorescently tagged microtubules through strong biotin−neutravidin linkages. Figure 2A gives the schematic diagram of the imaging setup. The fluorescence images of the microtubules (Figure 2B and movie 1 in the Supporting Information) were acquired with both excitation and emission at the coverslip side of the microchannel. The fluorescence image quality thus should not be affected by the presence of the microchannel. The 40 nm gold nanospheres were imaged with high contrast in DIC mode (Figure 2C), where the illumination beam passed through the entire thickness of the microdevice, including the PDMS slab portion. The gold nanospheres in the DIC images were localized with a precision of a few nanometers following the procedure outlined in the Supporting Information. Most of the single gold nanospheres fall no more than 40 nm (an average of 10 nm with a standard deviation of 12 nm) away from the center of the microtubule, suggesting that the DIC images were not affected by the presence of the channel. (See Figure S1 in the Supporting Information for the DIC image of the micronecklace together with the channel wall.)

DIC microscopy was purposely selected to show the undistorted images because the DIC image quality is highly dependent on the optical quality of the sample slide. In principle, DIC microscopy is a two-beam interferometer, in which an illumination beam is split into two orthogonally polarized beams, which are recombined after passing through the sample to generate an interference pattern. A small difference in the optical density on

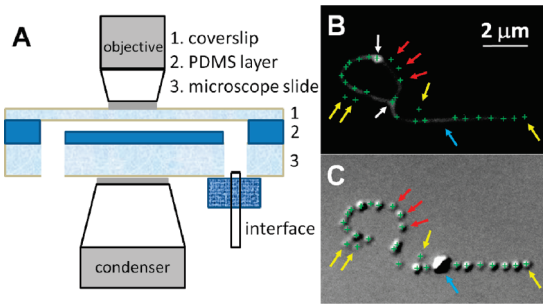

Figure 2. Localization of the 40 nm gold nanospheres bound to the microtubules in the channel. (A) Schematic diagram of the experimental setup. The microchannel is 5 μm deep and 25 μm wide. The PDMS layer sandwiched between the slide and coverslip is 60 μm thick. (B) Fluorescence image of the rhodamine-tagged microtubules. The gold nanospheres are invisible in this figure. The shape of this microneckalce is created randomly through multiple connection points (white arrows) where two or more microtubules are attached to the same gold nanospheres. (C) DIC image of the gold nanospheres. The mapped positions of the gold nanospheres are shown as green crosses on both fluorescence and DIC images. Three nanospheres (red arrows) are on a floating microtubule which is attached to the surface only at the two connection points. Movie 1 in the Supporting Information shows this microtubule moves while the other parts of the necklace do not move at all. Moreover, there is one aggregate (blue arrow) or a group of nanospheres that are located within distances smaller than the diffraction limit of light. Finally, some nanospheres (yellow arrows) are clearly separated from the microtubules by at least 600 nm. They were likely detached from the microtubules before the images were taken.

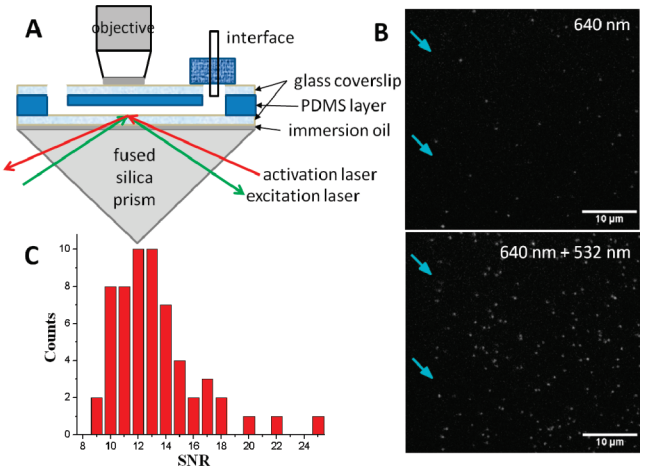

Figure 3. Activation and excitation cycles of single dye molecules in the microchannel. (A) Experimental setup of a home-built prism-type TIRFM operating with 532 nm and 640 nm lasers. (B) Optical switching of single Alexa Fluor 647 molecules immobilized on the channel surface. The arrows point out the channel edge. (C) Histogram of SNR of 60 molecules. The SNR is defined as the ratio between the peak intensity of a bright fluorescent spot and the standard deviation of the noise.

the two beam paths, e.g., ripples or unparallelness of the PDMS slab, will generate unwanted contrast or background noise in the final image. (In fact, the smeared DIC images of gold nanoparticles inspired this study of developing Hi-Fi imaging channels. A quantitative evaluation of the DIC image quality using contrast and background noise level is included as Figure S2 in the Supporting Information.)

It should be noted that the DIC imaging in PDMS-based channels has been reported before;[37,38] however, the image quality was limited by the thickness of the PDMS layer, and only the images of micrometer-sized cells were presented. Here for the first time, the high-quality images of single nanoparticles were achieved in the PDMS-based microchannels. The influence of the PDMS layer thickness on the DIC image quality is demonstrated in Figure S3 in the Supporting Information.

The optical switching of individual dye molecules is considered a prerequisite of STORM.[39] In a recent study, the direct observation of single dye molecule was demonstrated in a flow cell setup.[40] However, this has not been demonstrated so far in PDMS or glass/PDMS hybrid microchannels due to the difficulty in collecting sufficient photons emitted by individual fluorophores for nondistorted high-precision localization over a relatively high background, which is mainly caused by nonideal optical quality of conventional microchannels. In the present study, the activation-excitation cycle of individual dye molecules was successfully performed in the Hi-Fi optical imaging microchannels on a recently published automatic angle scanning prism-type TIRFM setup.[41] It is worth mentioning that the prism-type VA-TIRFM generally provides several benefits over its objective-based counterpart, such as a wider range of incident angles, higher accuracy in incident angle determination, less excitation light scattering, and lower cost.

The channel design for single-dye observation on prism-type TIRFM is different from the one shown in Figure 1. The schematic diagram of the imaging setup was shown in Figure 3A. Two coverslips, instead of one microscope slide and one coverslip, are used, and the channel is on the coverslip that sits on top of the prism. Fluorescence photons pass through the PDMS layer and the top coverslip before being collected by the microscope objective.

Movie 2 in the Supporting Information shows the on/off effect of the Alexa Fluor 647 dyes coated on the channel surface. The fluorescent dyes were first excited by a 640 nm continuous wave (CW) laser until they went into a dark state, then photoactivated by a 532 nm CW laser, and finally excited again by the 640 nm laser (Figure 3B). The cycle of excitation and activation was repeated many times. Exposure time for each frame was 50 ms. The SNRs of 60 randomly distributed molecules are in the range from 9 to 25 with the mean value at ~12 (Figure 3C). The fabrication method of the ultrathin PDMS layer clearly maintains the sensitivity for single fluorophore detection.

The new design is also useful for combinatorial microscopic imaging[42] where two or more microscopy modes of different configurations are combined to harvest information from varied physical properties of photons. Biomolecules of interest are often tagged with fluorescent dyes or quantum dots and detected by a fluorescence microscope to report their spatial and temporal distributions, while unstained biological samples are often imaged under a DIC microscope. The combination of these two modes allows the correlation of the target molecules with the structure and morphology of the biological sample in real time. These two modes are commonly used in the alternate manner, which severely hampers the temporal resolution necessary for imaging dynamic biological processes.

In this study, an upright microscope was used in both DIC and epi-fluorescence modes at the same time. The two modes have different illumination light sources but share the same microscope objective. The DIC and fluorescence images are collected through the same microscope objective, split, and projected onto the left and right halves of the same CCD camera. The DIC and

dx.doi.org/10.1021/ac201056z |Anal. Chem. 2011, 83, 5073–5077

fluorescence images can be simultaneously acquired at frame rates mainly limited by the signal strength. This dual-mode microscopy setup makes it possible to track fluorescent tags and plasmonic nanoparticles[12,13,43] simultaneously for greater versatility and flexibility in revealing complex biological events.

A simple demonstration is shown in Figure S4 in the Supporting Information, in which 80 nm gold nanospheres and 85 nm fluorescent nanoparticles immobilized on the channel surface were imaged on a single exposure. The fluorescent nanoparticles and gold nanospheres were introduced to different parts of the channels through laminar flow.

The true power of combining dual-mode DIC/fluorescence microscopy with the Hi-Fi imaging microchannel lies in the ability to precisely monitor time-dependent fast cellular dynamics under controllable stimuli. As a demonstration, A549 human lung cancer cells were plated and grown in a Hi-Fi imaging channel. The 85 nm fluorescent nanoparticle solution was then injected into the channel and incubated for 4 h in an incubator before observation. Figure S5 in the Supporting Information shows a DIC/fluorescence image of a cultivated, living cell. The full z-scan of the cell (movie 3 in the Supporting Information) clearly shows a large number of fluorescent nanoparticles were internalized and distributed inside the cell.

In summary, this study presents a new design of ultraflat, ultrathin, modular microfluidic devices that are of high fidelity in optical imaging and compatible with most modes of far-field optical microscopy. These microdevices can be fabricated from PDMS and standard microscope slides and coverslips. Additional functional components, such as on-chip pneumatic valves and pumps, may be integrated using multilayer soft lithography.[44] These microdevices allow simultaneous imaging of live cells, fluorescent tags, and plasmonic nanoparticle probes in combinatorial microscopy. The Hi-Fi optical imaging microchannels have potential for conducting time-dependent chemical and biological studies at the single molecule and nanoparticle level under continuous external perturbation.

■ ASSOCIATED CONTENT

Supporting Information. The experimental details, five supplementary figures, and three movies. This material is available free of charge via the Internet at http://pubs.acs.org.

■ AUTHOR INFORMATION

Corresponding Author
*E-mail: nfang@iastate.edu.

■ ACKNOWLEDGMENT

Y.L. and W.S. contributed equally to this work. This work was supported by the start-up funds from Iowa State University (microfabrication) and by U.S. Department of Energy, Office of Basic Energy Sciences, Division of Chemical Sciences, Geosciences, and Biosciences through the Ames Laboratory (optical imaging). The Ames Laboratory is operated for the U.S. Department of Energy by Iowa State University under Contract No. DE-AC02-07CH11358. Y.L. was also supported in part by "Fundamental Research Funds for the Central Universities, China" (Grants DUT10RC(3)92 and DUT11SM11). We specially thank Prof. David Chen of the University of British Columbia for his financial support to C.L.'s visit to Ames Laboratory.

■ REFERENCES

(1) Chalfie, M.; Tu, Y.; Euskirchen, G.; Ward, W. W.; Prasher, D. C. *Science* **1994**, *263*, 802–805.
(2) Tsien, R. Y. *Annu. Rev. Biochem.* **1998**, *67*, 509–544.
(3) Michalet, X.; Pinaud, F. F.; Bentolila, L. A.; Tsay, J. M.; Doose, S.; Li, J. J.; Sundaresan, G.; Wu, A. M.; Gambhir, S. S.; Weiss, S. *Science* **2005**, *307*, 538–544.
(4) Sperling, R. A.; Gil, P. R.; Zhang, F.; Zanella, M.; Parak, W. J. *Chem. Soc. Rev.* **2008**, *37*, 1896–1908.
(5) Villalobos, V.; Naik, S.; Piwnica-Worms, D. *Annu. Rev. Biomed. Eng.* **2007**, *9*, 321–349.
(6) Toprak, E.; Selvin, P. R. *Annu. Rev. Biophys. Biomol. Struct.* **2007**, *36*, 349–369.
(7) Wang, Y. X.; Shyy, J. Y. J.; Chien, S. *Annu. Rev. Biomed. Eng.* **2008**, *10*, 1–38.
(8) Joo, C.; Balci, H.; Ishitsuka, Y.; Buranachai, C.; Ha, T. *Annu. Rev. Biochem.* **2008**, *77*, 51–76.
(9) Huang, B.; Bates, M.; Zhuang, X. W. *Annu. Rev. Biochem.* **2009**, *78*, 993–1016.
(10) Hell, S. W. *Nat. Methods* **2009**, *6*, 24–32.
(11) Wang, G. F.; Stender, A. S.; Sun, W.; Fang, N. *Analyst* **2010**, *135*, 215–221.
(12) Sun, W.; Wang, G. F.; Fang, N.; Yeung, E. S. *Anal. Chem.* **2009**, *81*, 9203–9208.
(13) Wang, G. F.; Sun, W.; Luo, Y.; Fang, N. *J. Am. Chem. Soc.* **2010**, *132*, 16417–16422.
(14) Bates, M.; Huang, B.; Dempsey, G. T.; Zhuang, X. W. *Science* **2007**, *317*, 1749–1753.
(15) Rust, M. J.; Bates, M.; Zhuang, X. W. *Nat. Methods* **2006**, *3*, 793–795.
(16) Betzig, E.; Patterson, G. H.; Sougrat, R.; Lindwasser, O. W.; Olenych, S.; Bonifacino, J. S.; Davidson, M. W.; Lippincott-Schwartz, J.; Hess, H. F. *Science* **2006**, *313*, 1642–1645.
(17) Hess, S. T.; Girirajan, T. P. K.; Mason, M. D. *Biophys. J.* **2006**, *91*, 4258–4272.
(18) Gelles, J.; Schnapp, B. J.; Sheetz, M. P. *Nature* **1988**, *331*, 450–453.
(19) Nan, X. L.; Sims, P. A.; Xie, X. S. *ChemPhysChem* **2008**, *9*, 707–712.
(20) Whitesides, G. M. *Nature* **2006**, *442*, 368–373.
(21) El-Ali, J.; Sorger, P. K.; Jensen, K. F. *Nature* **2006**, *442*, 403–411.
(22) Yager, P.; Edwards, T.; Fu, E.; Helton, K.; Nelson, K.; Tam, M. R.; Weigl, B. H. *Nature* **2006**, *442*, 412–418.
(23) Brewer, L. R.; Bianco, P. R. *Nat. Methods* **2008**, *5*, 517–525.
(24) Chronis, N.; Zimmer, M.; Bargmann, C. I. *Nat. Methods* **2007**, *4*, 727–731.
(25) Taylor, A. M.; Blurton-Jones, M.; Rhee, S. W.; Cribbs, D. H.; Cotman, C. W.; Jeon, N. L. *Nat. Methods* **2005**, *2*, 599–605.
(26) Mudrakola, H. V.; Zhang, K.; Cui, B. *Structure* **2009**, *17*, 1433–1441.
(27) Cai, L.; Friedman, N.; Xie, X. S. *Nature* **2006**, *440*, 358–362.
(28) Le, N. C. H.; Yokokawa, R.; Dao, D. V.; Nguyen, T. D.; Wells, J. C.; Sugiyama, S. *Lab Chip* **2009**, *9*, 244–250.
(29) Foquet, M.; Korlach, J.; Zipfel, W.; Webb, W. W.; Craighead, H. G. *Anal. Chem.* **2002**, *74*, 1415–1422.
(30) Tan, X.; Mizuuchi, M.; Mizuuchi, K. *Proc. Natl. Acad. Sci. U.S.A.* **2007**, *104*, 13925–13929.
(31) Crane, M. M.; Chung, K.; Stirman, J.; Lu, H. *Lab Chip* **2010**, *10*, 1509–1517.
(32) Taniguchi, Y.; Choi, P. J.; Li, G. W.; Chen, H. Y.; Babu, M.; Hearn, J.; Emili, A.; Xie, X. S. *Science* **2010**, *329*, 533–538.
(33) Huang, B.; Wu, H. K.; Bhaya, D.; Grossman, A.; Granier, S.; Kobilka, B. K.; Zare, R. N. *Science* **2007**, *315*, 81–84.
(34) Pfeil, S. H.; Wickersham, C. E.; Hoffmann, A.; Lipman, E. A. *Rev. Sci. Instrum.* **2009**, *80*, 055105/1–055105/9.
(35) Lemke, E. A., Gambin, Y., Vandelinder, V., Brustad, E. M., Liu, H. W., Schultz, P. G., Groisman, A., Deniz, A. A., *J. Am. Chem. Soc.* **2009**, *131*, 13610.

(36) McDonald, J. C.; Duffy, D. C.; Anderson, J. R.; Chiu, D. T.; Wu, H. K.; Schueller, O. J. A.; Whitesides, G. M. *Electrophoresis* **2000**, *21*, 27–40.
(37) Shelby, J. P.; White, J.; Ganesan, K.; Rathod, P. K.; Chiu, D. T. *Proc. Natl. Acad. Sci. U.S.A.* **2003**, *100*, 14618–14622.
(38) Park, J. W.; Vahidi, B.; Taylor, A. M.; Rhee, S. W.; Jeon, N. L. *Nat. Protoc.* **2006**, *1*, 2128–2136.
(39) Heilemann, M.; van de Linde, S.; Schiittpelz, M.; Kasper, R.; Seefeldt, B.; Mukherjee, A.; Tinnefeld, P.; Sauer, M. *Angew. Chem., Int. Ed.* **2008**, *47*, 6172–6176.
(40) Wang, B.; Ho, J.; Fei, J. Y.; Gonzalez, R. L.; Lin, Q. A. *Lab Chip* **2011**, *11*, 274–281.
(41) Sun, W.; Marchuk, K.; Wang, G. F.; Fang, N. *Anal. Chem.* **2010**, *82*, 2441–2447.
(42) Axelrod, D.; Omann, G. M. *Nat. Rev. Mol. Cell Biol.* **2006**, *7*, 944–952.
(43) Stender, A. S.; Wang, G. F.; Sun, W.; Fang, N. *ACS Nano* **2010**, *4*, 7667–7675.
(44) Unger, M. A.; Chou, H. P.; Thorsen, T.; Scherer, A.; Quake, S. R. *Science* **2000**, *288*, 113–116.